XRF ANALYSIS - SOME SENSITIVITY COMPARISONS BETWEEN CHARGED-PARTICLE AND PHOTON EXCITATION*

F. S. Goulding and J. M. Jaklevic

Lawrence Berkeley Laboratory
University of California
Berkeley, California 94720 U.S.A.

SUMMARY

A comparison is made between the limits of detection for trace elements when charged-particle and photon excited X-ray fluorescence analysis are performed on a specific type of sample (5 mg/cm^2 organic based). Large-scale analysis (~ 30,000 samples per year) at levels of 1 ppm or lower is shown to be practical with either technique when well executed. Determining the physical reason for unexplained detector background is shown to be very important particularly for the potential improvement that might be realized in photon-excited analysis applications.

* This work was done with support from the U. S. Energy Research and and Development Administration under Interagency Agreement with the U. S. Environmental Protection Agency.

XRF ANALYSIS - SOME SENSITIVITY COMPARISONS BETWEEN CHARGED-PARTICLE AND PHOTON EXCITATION

F. S. Goulding and J. M. Jaklevic

Lawrence Berkeley Laboratory
University of California
Berkeley, California 94720 U.S.A.

1. INTRODUCTION

A direct comparison of the sensitivities for trace element measurements using either charge-particle or photon excited XRF analysis is made difficult by the fact that each has particular relevance to certain applications, and its performance is related to the type (particularly size) of sample. However, the paper by Folkmann et al[1] has placed charged-particle excitation on a firm theoretical and experimental basis, and this work can be used to extrapolate to a variety of cases. The present authors reported[2] similar calculations to those of Folkmann, but an unduly pessimistic prediction of sensitivity for a given measurement time resulted from a conservative estimate of the allowable beam intensity and from a significant error in the calculation. We have now repeated the calculations and are largely in agreement with Folkmann. The purpose of this paper is to present data on an optimum photon-excited XRF system and to discuss the theoretical and experimental sensitivity limits of this method.

In order to compare the performance with the charged particle results of Folkmann, we will standardize on samples mainly of organic (i.e., carbon) content and weighing 5 mg/cm^2. This is typical of the filters used to collect air particulates. We will also assume that large-scale analysis of samples is required, so the analysis time per sample for the 30 or so elements generally analyzed by these systems will be restricted to less than 10 minutes. This corresponds to comfortably handling 30,000 samples per year.

2. SENSITIVITY OF PARTICLE-INDUCED X-RAY EMISSION ANALYSIS

The limit to sensitivity (detection limit) of any measurement system is set by statistical fluctuations in the background that conceal weak signals. In this study of X-ray fluorescence systems, we will adopt the convention that the detection limit for a particular X-ray spectral peak is equal to $3\sqrt{B}$ where B is the spectral background in the peak region integrated over the width of the peak. A better limit might be $3.29\sqrt{B}$ corresponding to the 95% confidence limit but $3\sqrt{B}$ is more commonly employed in the literature but the difference is negligible for our purpose.

Charged particle excitation involves the ejection of electrons from the appropriate shell(s) of the constituent atoms by collision with charged particles travelling through the sample. The subsequent filling of the shells causes emission of X-rays characteristic of the elements in the sample. The main background, particularly at low X-ray energies, arises from bremsstrahlung produced in the sample by the electrons ejected mainly from the carbon matrix. Note that the same basic process produces both the low-energy background and the characteristic X-rays of elements of interest. Background at higher X-ray energies is partly due to bremsstrahlung produced by the particle itself, but is often dominated by nuclear reactions in the sample which produce gamma-rays that cause a Compton electron distribution in the detector.

The process of the ejection of electrons from atoms by passage of charged particles can be analyzed using the Born approximation or the classical binary-encounter collision model discussed by Garcia[3]. The latter method must be modified to take into account the distribution of velocities of electrons in the various shells[4] in order to avoid false behavior for

high-ejected electron energies. These calculations form the basis of Folkmann's work, and they permit a good estimate of both X-ray production cross sections and the secondary-electron bremsstrahlung production. Folkmann also calculates the particle bremsstrahlung. From these calculations, backed by experimentally measured cross sections, he has produced sensitivity curves for various energies of protons.

In order to present his results in a form directly comparable to that to be given for photons, it is necessary to define the conditions of the exposure and the size of sample. Work by a number of groups suggests that a 100 nA beam current (protons) spread over an area approaching 1 cm^2 is acceptable from the point of view of sample heating. Since it is common to use two beam energies (with absorbers) to optimize performance for a range of elements, we will assume a counting time of 200 sec for each energy. This corresponds to a total charge of 20 μC at each beam energy on the sample of 5 mg/cm^2 assumed for the purpose of comparison in this paper. It is also necessary to define the efficiency of the sample-detector geometry (assuming the detector is 100% efficient for the X-rays of interest). We will assume the value (0.3% geometrical efficiency) used by Folkmann. With these assumptions, the electron and proton bremsstrahlung and the yield of X-rays of elements present at the 1 ppm level can be calculated. Figures 1 and 2 show the results for 2 MeV and 4 MeV protons. We have selected these energies for this comparison because they are reasonably optimum for realizing good sensitivity over the whole range of interesting elements and the ions have adequate range so that we can neglect the loss of particle energy in traversing the sample. Note that the X-ray yields given on these figures include the effect of vacancy-filling by Auger electron emission which results in a fluorescent yield of X-rays well below unity, becoming very

small for low-Z elements. The detection limit for a particular element is easily determined, knowing both the background B counts at the energy of the X-ray line and the number of counts S of elemental X-rays in the line. Thus

$$\text{Detection Limit } C_o \text{ (ppm)} = \frac{3\sqrt{B}}{S} \qquad (1)$$

Table 1 shows the detection limits calculated by this method for some selected elements

The detection limits derived by this method are subject to some questions. At the higher energies the number of counts in an X-ray peak is extremely small, and it is unrealistic to quote a limit in which the actual number of counts is hardly statistically meaningful. Also, production of background at high energies by nuclear reactions may be expected to be quite sensitive to the composition of the sample, and this may add to uncertainties for high-energy peaks. At the lower energies the rapidly rising background is not ideal for computer background subtraction, so some loss of sensitivity may result here too. Pulse pile-up may also be an important problem in some experimental systems. Finally the tight geometry used by Folkmann (0.3% efficiency) may sometimes be unrealistic and numbers ~ 10 times smaller are often used.

In keeping with these reservations, experimental results[5-8] analyzed by the authors generally appear to be higher than the calculated limits, but not by a large factor (say < 10). Therefore, detection limits of approximately 1 ppm or smaller appear to be feasible using such short charged-particle excitation periods. It is also quite clear from Fig. 2 that use of two or more energies together with appropriate absorbers to cut the high counting rates at low energies is essential for achieving good sensitivity over the range of interesting elements.

TABLE 1

Charged particle excitation calculated detection limits (3 σ) in ppm by weight (20 μC beam, 5 mg/cm^2 sample, solid angle 4π x 0.003 sr Geom)

Element	2 MeV p's	4 MeV p's
S	0.24	
Ca	0.27	
Fe	0.05	0.25
Zn	0.04	
Pb (Lα)	0.24	0.21
Br	0.07	0.05
Mo	0.26	0.06
Cd	1.23	0.13

3. SENSITIVITY OF PHOTON-INDUCED X-RAY EMISSION ANALYSIS

In this case, we will focus discussion on a system developed[9] for the large-scale analysis of air pollution filters. The system uses a pulsed X-ray tube[10] with a tungsten anode to produce a broad-band X-ray spectrum which excites one of three computer-selectable targets (Ti Kα - 4.5 keV; Mo Kα = 17.5 keV; Sm Kα = 40 keV) whose characteristic radiation illuminates the sample. The sample is normally a very clean cellulose acetate filter on which air particulates have been deposited. The mass of the filters is generally 5 mg/cm^2 although thinner substrates are sometimes employed. X-rays from the samples are analyzed by a guard-ring reject detector system[11] which provides a very low background while maintaining an efficient geometry

(see Fig. 3). Similar performance can be attained insofar as sensitivity is concerned by using a standard type of silicon detector and a highly collimated X-ray geometry to prevent X-rays from reaching regions near the periphery of the detector. Such a system, however, requires a high-power X-ray tube (~ 3 KW) which we avoid by using the guard-ring detector.

The system operates at a useable output counting rate in excess of 10 Kc/s. This output rate, which is far in excess of that achieved by most XRF systems, is a direct result of the pulsed X-ray method. A sample is subjected to excitation by each of the three targets in turn; typically the Ti target is employed for 100 sec, molybdenum for 100 sec and samarium for 200 sec to achieve reasonably uniform sensitivity for about 30 interesting elements. The total counting time per sample is therefore the same as we allowed in discussing particle-induced X-ray emission analysis.

The absorption of photons to create vacancies in the atomic shells of elements has received much theoretical study. The theoretical results, together with extensive experimental data, are combined in comprehensive X-ray cross section data compilations[12] which will be used here to predict the efficiency for X-ray production in various elements by the incident radiation on the sample. It is also necessary to know the fluorescent yield (i.e., the fraction of shell-vacancy fillings accompanied by X-ray emission) for the K shells of light elements and the L shells of heavy elements since these are the X-rays used in XRF analysis. The review paper by Bambynek et al[13] is used as the source for fluorescent yield data and for the relative yields of different K or L X-ray lines. Using these two sets of data, reasonably accurate predictions can be made of the characteristic X-ray output rate for various elements when a sample is irradiated with photons of known energy.

It is also possible to use X-ray cross-section data tables to determine the amount of scattering (both Rayleigh and Compton) of incident photons from the sample to the detector and thereby to predict the counting rate in the scatter peaks that appear at the high energy end of the spectrum observed by the detector. Examples of the spectra produced by the analysis system for each secondary target are shown in Figs. 4, 5 and 6. The main features of these spectra are the scatter peaks at high energy and the characteristic lines of the various elements--both predictable--and a rather flat background whose behavior will now be discussed.

The background observed in these spectra might be expected to arise from four sources:

1) Bremsstrahlung radiation produced by secondary electrons in the sample caused primarily by photoelectric interactions of the incident X-rays with atoms of the main constituent (i.e. carbon).

2) Escape mechanisms in the detector. These could involve both the escape of photoelectrons produced in the detector and the emission and escape of bremsstrahlung photons produced by these electrons. Note that silicon K X-ray escape would cause spurious weak peaks just below strong spectral features, but could not contribute a general background.

3) Poor charge collection in the detector. This involves the loss of holes and/or electrons as they are collected by the electric field in the detector. However, to explain the spectral background shape, the loss of amounts of charge ranging from zero to the full amount for different events must occur.

4) Defects in the electronic signal processing chain.

We believe that 4) can be completely eliminated as a possible source of background in our system since a test pulser causes no background under realistic operating conditions. The charge-loss effect is certainly present when photons irradiate the whole of a simple detector. The amount of background due to this is known to be influenced by chemical treatment of the detector surface, and the effect has been shown to be due to the electric field distortions caused in the bulk by surface channels on the detector[14]. However, we also know that the surface-dependent background can be eliminated by use of the guard-ring reject method[11] or by collimating X-rays to avoid their interacting in regions of the detector affected by surface channels. Therefore, use of good experimental techniques should result in elimination of surface effects as a source of charge loss. It is intuitively obvious that bulk charge loss is unlikely to exhibit the characteristic of losses varying from zero to full charge with the majority of events experiencing no loss whatsoever. Therefore, we are strongly inclined to dismiss both items 3) and 4) as candidates to explain our background. A further pointer in this direction is the observation that the background we observe in detector testing is virtually constant from detector to detector* and does not exhibit the variations that might be expected if material properties or surface conditions were important. This observation points to a fundamental physical cause of the background.

The most obvious physical cause of background in XRF is the bremsstrahlung radiation produced by secondary electrons in the sample. This effect is calculated in Appendices I and II, and the results of the calculations

* To be valid this test must be performed on a guard-ring detector or a simple detector with X-rays collimated to avoid the periphery.

are shown in Figs. 4, 5 and 6 to be discussed later. However, two experimental tests can easily be performed which show that most of the observed background does not arise from the sample. If it did, interposing a filter (e.g., Cu) in the path between sample and detector should produce a notch in the background--this does not happen. Furthermore, detector tests with radioactive sources (e.g., ^{109}Cd) exhibit a similar ratio of the total background counts to the counts in high-energy peaks as is observed in XRF experiments. The integrated number of background counts is ~ 2 to 8% of the total number of high-energy counts depending on the energy of radiation incident on the detector.

These observations lead to the inescapable conclusion that the background is primarily due to a basic physical mechanism in the detector which produces the escape of a substantial fraction of the energy in ~ 5% of the cases of photons interacting in the detector. A simple computation in the case of ^{109}Cd radiation (22 keV) shows that the loss would correspond to every event in a 30 μm layer at the front face of the detector losing part of its energy. In Appendices III and IV maximum values for the losses due electron and bremsstrahlung escape are calculated. As might be expected from simple considerations of the range of 22 keV electrons (~ 2 μm), and of the low probability of bremsstrahlung production, normal treatments of these two terms do not predict the background behavior observed in detectors. Appendix V examines other alternative possibilities, which prove to be much too small. Also, known dead layers at the front surfaces of silicon detectors are < 0.3 μm thick, and charge losses in these dead layers are far smaller than needed to explain the background level.

For the present, we are forced to accept the existence of an unknown physical mechanism that produces background extending from the position of high-energy peaks in a spectrum down to zero energy. Possibly this could be an electron channeling mechanism[15] that increases the escape range of electrons in the single-crystal silicon detector. However, our experiments to date have not confirmed such a mechanism.

Figures 4, 5 and 6 show a set of typical x-ray spectra generated by the system when analyzing an air-particulate filter. These figures illustrate the value of using the three targets to excite the sample and thereby to produce reasonably uniform sensitivity over a broad energy range. Table 2 shows the analysis results for this particular filter. The results are normally expressed in ng/cm^2 of each element, but since most of the background arises in the detector due to degraded scattered photons from the cellulose acetate filter medium (5 mg/cm^2), it is best for comparison purposes to express the results in ppm by weight. These results are shown in the last column of Table 2.

TABLE 2

Measured elemental compositions (see Figs. 4, 5 and 6)

Element	Conc (ng/cm^2)	ppm by weight
Si*	282	56
S *	11600	2320
Cl*	85	17
K	224	45
Ca	192	38
Fe	344	69
Cu	76	15
Zn	485	97
Se	7	1.4
Br	105	21
Pb	627	125
Cd	23	4.6
Sn	29	5.8

* A 50 μm Be window present in this particular system causes substantial reductions (~ 2 to 3 times) in the intensity of these lines in the spectrum.

As indicated earlier, we can also predict the yields of various elemental X-rays from published data compilations and normalize these yields in terms of the backscattered photons produced mainly by the organic matrix. With the assumption that both the characteristic X-rays and the scattered radiation are distributed isotropically (not valid, but acceptable for an initial guess under most experimental conditions), this permits an estimate of the number of characteristic X-rays registered by the detector per backscattered photon detected. In Figs. 7, 8 and 9, data are presented which shows the yield of characteristic (mainly Kα) X-rays produced by 1 ppm (by weight) of selected elements when 10^6 backscattered photons are detected.

These figures also show the calculated sample bremsstrahlung background and the actual measured detector background (in the guard-ring reject mode). As discussed earlier, this background far exceeds the predictable amounts, but, for the present, we are forced to accept this high level. Since all backgrounds in Figs. 7, 8 and 9 are expressed in terms of the amount /200 eV for 10^6 backscatter counts, and the various elemental yields shown in these figures are spread over a system resolution of about 200 eV, and are also expressed for 10^6 backscatter counts, a direct comparison between the counts in a peak and the background under it can be made. In the case of our system, when the counting rate of 10 kc/s is due almost entirely to the backscatter peaks, it can be shown that the 3σ concentration detection limit Co is given by:

$$C_o = \frac{30}{S}\sqrt{\frac{B}{T}} \qquad (2)$$

where S is the signal (i.e., counts) in a 1 ppm peak

B is the background at the peak position

T is the counting time (sec)

(all derived from Figs. 4, 5 or 6)

Calculated detection limits for selected elements are shown in Table 3. Measured values achieved in routine use of the system are also shown. The agreement is quite good, which is not really surprising since an experimentally measured detector background was used in deriving the calculated values. Probably the main discrepancy between the two sets of numbers arises from inadequate knowledge for the angular distribution of scattered radiation.

We note that detection sensitivities could be improved by factors ranging from 2 to 20 times if the unknown source of detector background could be eliminated. This places a great deal of emphasis on understanding the unknown background source and removing it if possible.

TABLE 3

Photon excitation calculated and experimental detection limits (ppm by weight)

Element	Calculated	Measured
+ Al	8.2	8.2*
+ S	2.7	2.6*
+ Ca	1.7	-
Δ Fe	1.3	1.8
Δ Zn	0.6	1.1
Δ Br	0.4	0.5
Δ Pb (Lβ)	0.9	1.5
o Mo	1.0	-
o Cd	0.7	0.9

\+ TiK X-ray Excitation for 100 sec
Δ MoK X-ray Excitation for 100 sec
o SmK X-ray Excitation for 200 sec
* These numbers are measured values corrected for window absorption between sample and detector.

4. DISCUSSION

The results presented in this paper indicate that, for this type of sample, the detection limits achieved by the two methods in practice are very similar but a small advantage is predicted for particle-induced X-ray method under ideal circumstances. This conclusion might change for other types of sample but probably not very much. It is also apparent that, if the unknown source of detector background could be eliminated, the sensitivity of the photon-induced X-ray method could be significantly improved. Either method can, in principle, meet the need for large-scale analysis of samples for elemental levels of approximately 1 ppm by weight. If longer analysis times are allowed, the sensitivity can be improved accordingly.

The choice between the two methods is, therefore, likely in many cases to rest on other considerations, such as availability, reliability, cost and portability. Anticipated large-scale applications (e.g., in hospitals) will probably favor the photon method because it must certainly be rated the best in these respects. However, where an accelerator is available, specific advantages of the charged-particle method, such as its potential to analyze very small samples and the ability to selectively analyze surfaces, can be valuable. The ability to scan samples with a fine particle beam would also be a very useful analytical feature.

5. ACKNOWLEDGMENTS

This paper was stimulated by the work of Dr Finn Folkmann, who drew our attention to a mistake in our earlier analysis of the charged particle method. The experimental results on photon excitation were obtained by

Billy Loo and Ray Gatti and are representative of many thousands of samples analyzed by them on equipment assembled by Bill Searles, Norman Madden, Donald Landis and Dick Adachi. The data on detector characteristics are the result of work by Jack Walton and Heinrich Sommer.

APPENDIX I

Bremsstrahlung Production by Electrons

According to Heitler[16] the cross section for an electron of energy E(keV) producing a photon of energy between E_x(keV) and $E_x + dE_x$(keV), where $E_x < E$ is given by:

$$\sigma_{E \to E_x} \approx 1.5 \times 10^{-24} \frac{Z^2}{E} \left\{ \frac{dE_x}{E_x} \right\} \text{cm}^2/\text{atom} \qquad (3)$$

where Z is the atomic number of the absorber.*

Also, using the Bethe-Bloch relationship, we can show that the loss of energy by an electron along its path is represented by:

$$\frac{dE}{dx} \approx \frac{38.4}{E} \ln \left\{ \frac{100E}{Z} \right\} \text{keV per mg/cm}^2 \qquad (4)$$

Since the logarithmic term here varies only slowly with energy, this relationship can be simplified in practice to:

$$\frac{dE}{dx} \approx \frac{180}{E} \text{keV per mg/cm}^2 \qquad (5)$$

or

$$dx \approx 1.67 \times 10^{18} \frac{E}{Z} dE \text{ atoms/cm}^2 \qquad (6)$$

---

* The Heitler relationship cannot apply exactly to this case according to Ishii and Morita[17] but the alternative equations do not lend themselves to simple analytical use. Therefore, since the results achieved using the simple approach appear to agree reasonably with experiment, we shall continue to use the Heitler relationship here.

This equation provides an estimate of the distance traveled by an electron of energy E while losing energy dE. By combining Eqs. (3) and (6), we can find the probability P that an electron losing energy dE by other absorption processes, such as ionization, will emit a bremsstrahlung photon whose energy lies between E_x and $E_x + dE_x$. Thus:

$$P = 2.5 \times 10^{-6} Z \left\{\frac{dE_x}{E_x}\right\} dE \qquad (7)$$

This result is independent of the actual electron energy providing that $E > E_x$. Therefore, if an electron of initial energy E_o is produced in an absorber, the total probability P_x that it will emit a bremsstrahlung photon in the energy range E_x to $E_x + dE_x$ while slowing down to energy E_x is given by:

$$P_x = 2.5 \times 10^{-6} Z \left\{\frac{dE_x}{E_x}\right\} (E_o - E_x) \qquad (8)$$

Fortunately, bremsstrahlung emission is a rare process so the energy losses due to it can be neglected when considering the range-energy relationship for a large population of electrons.

APPENDIX II

Photon Excitation: Ratio of Bremsstrahlung to Scattered Photons From Sample

Interactions of incident photons in a carbon matrix are predominantly photoelectric when the photons are of the low energies typically used in X-ray fluorescence analysis. At somewhat higher incident energies (e.g., 40 keV) sometimes employed, Compton scattering becomes important, but the maximum energy that can be acquired by an electron in the sample in Compton

collisions is quite low. Therefore, it is a fair assumption that significant bremsstrahlung background in the energy range where interference with trace element lines might occur arises from photoelectrons whose initial energy can, for practical purposes, be taken as that of the incident photons. Therefore, Eq. (8) can be used directly to predict the bremsstrahlung production in the sample. If the sample thickness t (g/cm^2) is small compared with the absorption length for photons of interest (not always a valid assumption) and if the photoelectric cross section of the matrix at the incident X-ray energy E_x is σ_{IP} (cm^2/gm), the number of photoelectrons produced is given by:

$$N = N_I \sigma_{IP} t \tag{9}$$

where N_I is the total number of incident photons.

Using Eq. (8) we find that N_x photons of energy E_x to $E_x + dE_x$ will be emitted from the sample where N_x is given by:

$$N_x = 2.5 \times 10^{-6} Z N_I \sigma_{IP} t \left\{\frac{dE_x}{E_x}\right\}(E_I - E_x) \tag{10}$$

It is convenient to normalize the background in terms of the number of counts in the detector caused by scatter from the sample (Rayleigh + Compton). While the scattered radiation is not distributed isotropically, typical detector-source-sample geometries are such that the scattered radiation reaching the detector can roughly be determined by assuming only isotropic Compton scatter. This is convenient since it permits an estimate of the ratio of bremsstrahlung (isotropic) reaching the detector to the scattered radiation that is independent of the precise geometry. If N_s is the number of scattered photons and σ_{IC} is the Compton cross section (g/cm^2), we have

$$N_S = N_I \, t \, \sigma_{IC} \tag{11}$$

The ratio N_X/N_S is therefore given by:

$$\frac{N_x}{N_s} = 2.5 \times 10^{-6} \, Z \, \frac{\sigma_{IP}}{\sigma_{IC}} \left\{ \frac{E_I - E_x}{E_x} \right\} dE_x \tag{12}$$

where all energies are expressed in keV.

This relationship is the basis for the curves presented in Figs. 4, 5 and 6 for three different energies of excitation. It is also of interest to determine the relative total number of counts in the background compared with the scatter peaks. This can be evaluated by integrating Eq. (8) with the bottom limit of integration chosen to avoid the pole which occurs in Eq. (8) at $E_X = 0$. This is reasonable since low-energy bremsstrahlung photons are absorbed both by the sample and by the detector system window. Using E_I/n as the lower limit we have:

$$F = \frac{\text{Total Sample Bremsstrahlung}}{\text{Total Scatter}} = 2.5 \times 10^{-6} \, \frac{\sigma_{IP}}{\sigma_{IC}} \, ZE_I \left[\ln(n) + \frac{1}{n} - 1 \right] \tag{13}$$

The value of F in carbon evaluated for Sm Kα radiation is 0.005%, for Mo Kα it is 0.072% and it increases to 1.9% for Ti Kα radiation (assuming n = 10). These numbers compare with the several percent actually measured as background in an XRF system.

APPENDIX III

Bremsstrahlung Escape From The Detector

The purpose of this Appendix is to eliminate the possibility that bremsstrahlung escape from the detector can be the source of the background observed in silicon detectors. A detailed analysis of these losses is made difficult by the fact that escape can take place at all detector surfaces; however, the following argument will show that the loss of every energetic ($E > E_I/10$) bremsstrahlung photon produced in the detector would be far from capable of explaining the few percent loss required to explain detector background. According to Eq. (8) of Appendix I:

$$P_x = 2.5 \times 10^{-6} Z \left\{ \frac{E_o}{E_x} - 1 \right\} dE_x$$

Assuming that the incident photons are all of energy E_I (the scatter peak energy) and that they produce photoelectrons of energy E_x, Eq. (8) can be integrated to give the total probability P_T of emission of photons of energies ranging from E_I shown to E_I/n. Thus:

$$P_T = 2.5 \times 10^{-6} Z E_x [\ln(n) + 1/n - 1] \qquad (14)$$

For $Z = 14$ (silicon), $E_I = 20$ keV and $n = 10$: $P_T = 10^{-3}$.

This is far below the observed background. Moreover, it is clear that the bremsstrahlung losses would be much less than this number because many of these photons would be absorbed in the detector and form part of full-sized signals.

APPENDIX IV

Electron Escape From The Detector

For the purpose of this discussion, we will assume that the silicon acts as a "normal" absorber and neglect any possibility that absorption is affected by channeling effects in the single crystal. Again, as in the previous Appendix, a maximum value for the losses will be calculated. Eq. (5) of Appendix I can be integrated to give a rough estimate of the "random walk" range R of an electron of energy E_I produced by the incident radiation. Thus:

$$R = \frac{E_I^2}{360} \text{ mg/cm}^2 \qquad (15)$$

For silicon and for E_I = 20 keV this corresponds to approximately 4 μm. The actual distance beneath a surface from which an electron might escape is much smaller than this--say 2 μm. Since the fraction of 20 keV incident X-rays absorbed in a 2 μm layer of silicon is only 0.2%, this escape mechanism clearly cannot explain the detector background. For 5 keV X-rays the loss becomes a maximum of 0.8%, still well below the observed background level.

APPENDIX V

Other Possible Background Sources

1) Secondary electrons from beryllium window

Even with the assumption that every electron produced by the radiation absorbed in a 10 μm layer of Be reached the detector and caused degraded signals, only a 0.006% contribution to background would result for 20 keV incident photons.

2) Secondary electrons from gold surface barrier layer

Assuming a 200 Å gold layer and that 50% of the photoelectrons produced in it causes degraded detector signals, a background contribution of 0.15% would result for 20 keV incident photons. In practice, many more photoelectrons would be lost and the effect would be even smaller.

REFERENCES

1) F. Folkmann, G. Gaarde, T. Huus and K. Kemp, Nucl. Instr. and Meth. 116 (1974) 487.

2) F. S. Goulding and J. M. Jaklevic, Ann. Rev. Nucl. Sci. 23 (1973) 45.

3) J. D. Garcia, R. J. Fortner and T. M. Kavanagh, Rev. Mod. Phys. 45 (1973) 111.

4) M. E. Rudd, D. Gregoire and J. B. Crooks, Phys. Rev. A. 3 (1971) 1635.

5) T. B. Johansson, R. E. Van Grieken, J. W. Nelson and J. W. Winchester, Anal. Chem. 47 (1975) 855.

6) V. Valković, et al., Nucl. Instr. and Meth. 114 (1974) 124.

7) P. J. Clark, G. F. Neal and R. O. Allen, Anal. Chem. 47 (1975) 650.

8) M. Barrette, et al., Nucl. Instr. and Meth. 134 (1976) 189.

9) R. L. Walter, R. D. Willis, W. F. Gutknecht and J. M. Joyce, Anal. Chem. 46 (1974) 843.

10) J. M. Jaklevic, D. A. Landis and F. S. Goulding, IEEE Trans. Nucl. Sci. NS-19 (1972) 392.

11) F. S. Goulding and J. M. Jaklevic, "Trace Element Analysis by X-ray Fluorescence", Lawrence Berkeley Laboratory Report No. UCRL-20625.

12) W. H. McMaster, N. Kerr Del Grande, J. H. Mallet and J. H. Hubbell, Lawrence Livermore Laboratory Report No. UCRL-50174.

13) W. Bambynek, et al., Rev. Mod. Phys. 44 (1972) 716.

14) F. S. Goulding, J. M. Jaklevic, B. V. Jarrett and D. A. Landis, Adv. X-ray Anal. 15 (1972) 470.

15) I. Bergström and B. Domeij, Nucl. Instr. and Methd. 430 (1966) 146.

16) W. Heitler, "The Quantum Theory of Radiation" (Clarendon, Oxford, 1954).

17) K. Ishii and S. Morita, Phys. Rev. A. 13 (1976) 131.

FIGURE CAPTIONS

Fig. 1. Calculated performance data for 2 MeV proton excitation (20 μC) on a 5 mg/cm^2 sample. The detector solid angle is assumed to be 4π x 0.003 sr. Electron and proton bremsstrahlung are shown together with the counts expected for 1 ppm (by weight) level of various trace elements. This data is derived from Folkmann's work and has been checked by calculation.

Fig. 2. As Fig. 1, but for 4 MeV proton excitation.

Fig. 3. The geometrical arrangement of the X-ray tube anode, secondary target (fluorescent), sample and detector used in the photon-excited system discussed in the paper. The tight geometry permits the use of a low power X-ray tube (< 100 W).

Fig. 4. A typical 5 mg/cm^2 air filter spectrum produced using Tk K (~ 4.5 keV) X-ray excitation--see Table 2 for elemental concentrations (75 sec counting time).

Fig. 5. Similar to Fig. 4, but using Mo K (~ 17.5 keV) X-ray for excitation.

Fig. 6. Similar to Fig. 4, but using Sm K (~ 40 keV) X-ray for excitation and with counting time increased to 250 sec.

Fig. 7. Calculated sample bremsstrahlung background and X-ray yields for 1 ppm (by weight) levels of selected trace elements. Also shown in the measured detector background curve. All are presented for 10^6 counts in the scatter peaks. This data is for Ti K X-ray excitation.

Fig. 8. Similar to Fig. 7, but for Mo K X-ray excitation.

Fig. 9. Similar to Fig. 7, but for Sm K X-ray excitation.

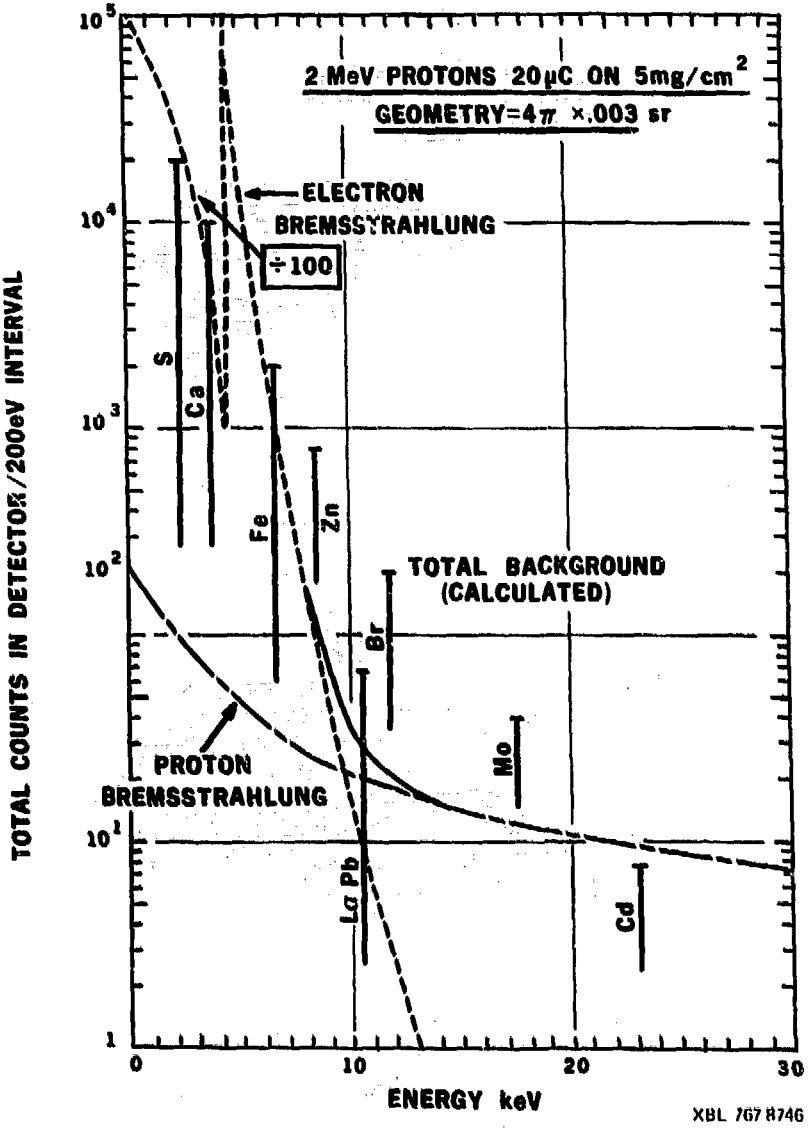
2 MeV PROTONS 20μC ON 5mg/cm²
GEOMETRY=4π ×.003 sr
ELECTRON BREMSSTRAHLUNG
÷100
TOTAL BACKGROUND (CALCULATED)
PROTON BREMSSTRAHLUNG
S
Ca
Fe
Zn
Br
Mo
La Pb
Cd
TOTAL COUNTS IN DETECTOR/200eV INTERVAL
ENERGY keV
XBL 767 8746

Fig. 1

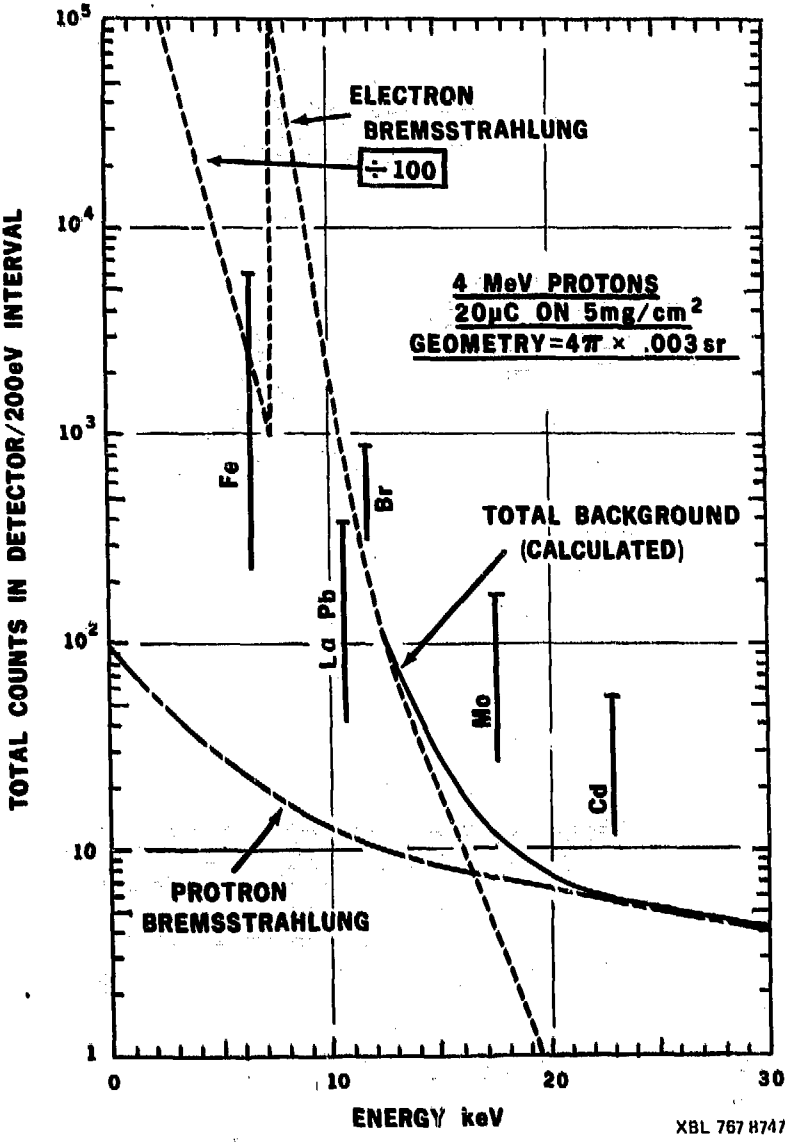
ELECTRON
BREMSSTRAHLUNG
÷100
4 MeV PROTONS
20μC ON 5mg/cm²
GEOMETRY=4π × .003 sr
TOTAL BACKGROUND
(CALCULATED)
PROTRON
BREMSSTRAHLUNG
Fe
La Pb
Br
Mo
Cd
TOTAL COUNTS IN DETECTOR/200eV INTERVAL
ENERGY keV
10⁵
10⁴
10³
10²
10
1
0
10
20
30
XBL 767 8747

Fig. 2

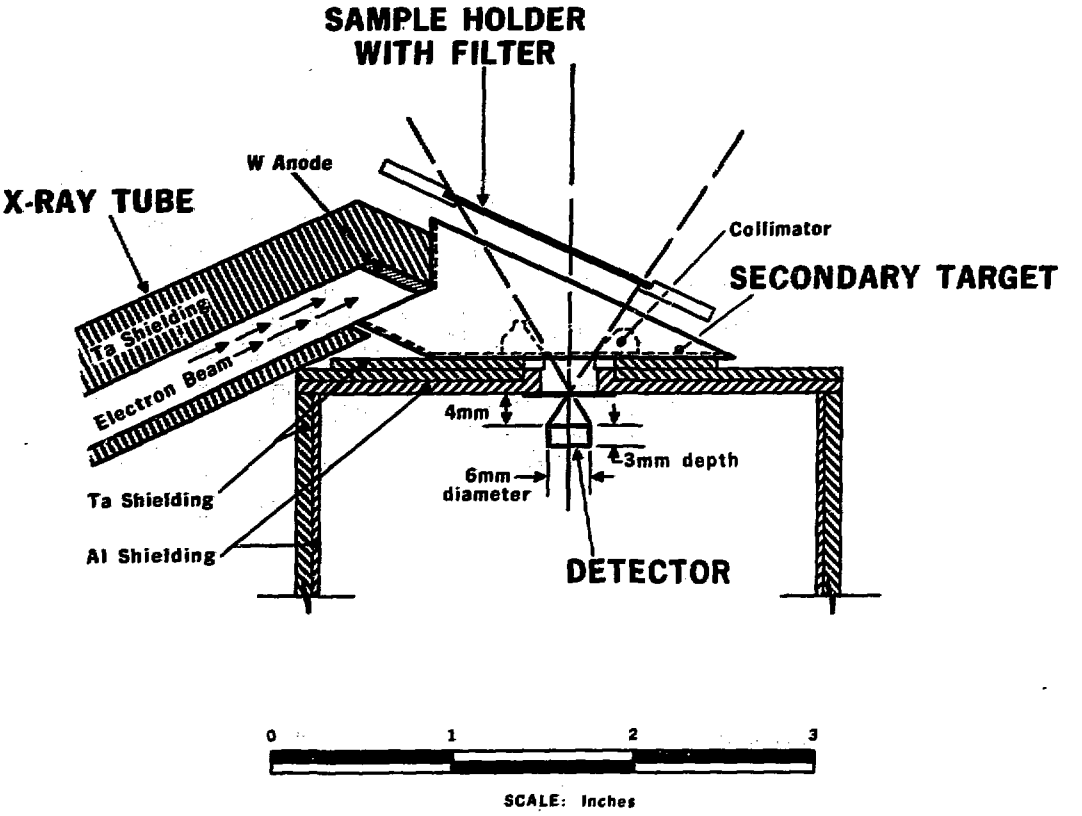

XBL 731-102

Fig. 3

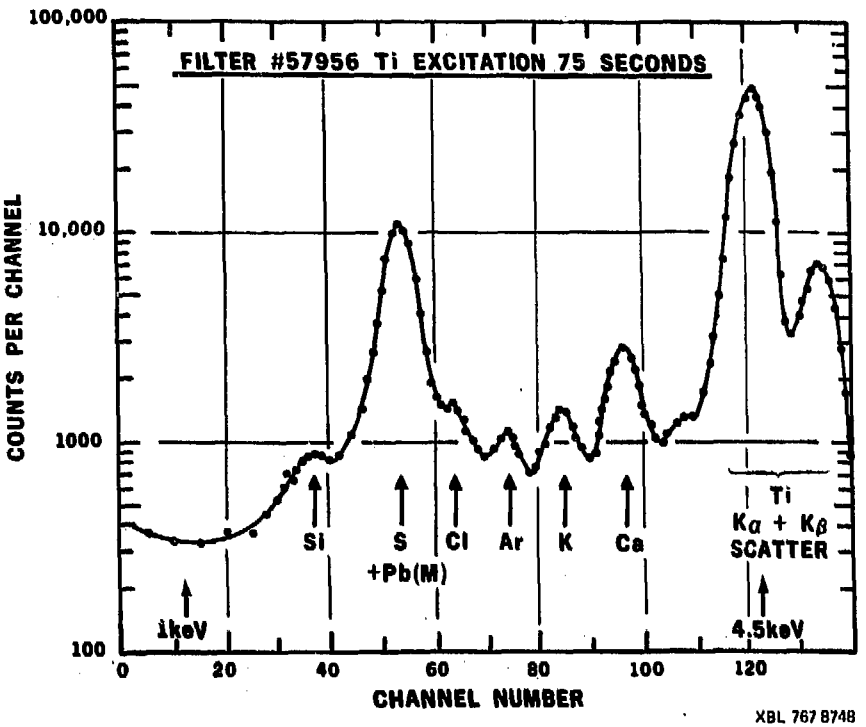
FILTER #57956 Ti EXCITATION 75 SECONDS
COUNTS PER CHANNEL
100,000
10,000
1000
100
0
20
40
60
80
100
120
CHANNEL NUMBER
1keV
Si
S
+Pb(M)
Cl
Ar
K
Ca
Ti
Kα + Kβ
SCATTER
4.5keV
XBL 767 8748

Fig. 4

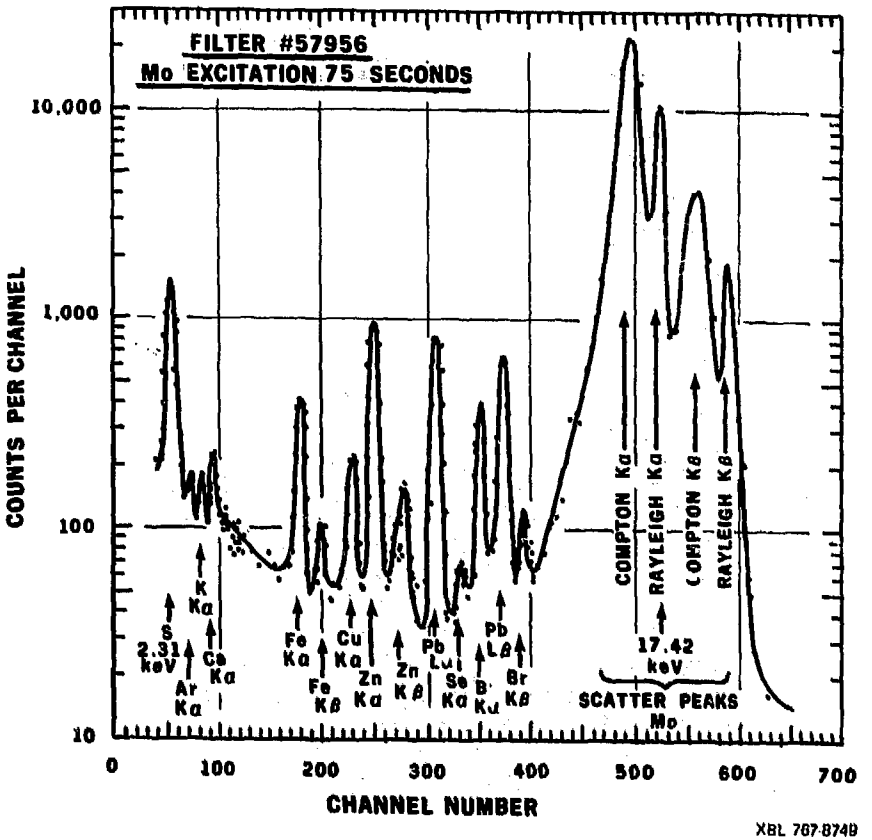
FILTER #57956
Mo EXCITATION 75 SECONDS
COUNTS PER CHANNEL
10,000
1,000
100
10
0
100
200
300
400
500
600
700
CHANNEL NUMBER
S 2.31 keV
Ar Kα
K Kα
Ca Kα
Fe Kα
Fe Kβ
Cu Kα
Zn Kα
Zn Kβ
Pb Lα
Se Kα
Br Kβ
Pb Lβ
COMPTON Kα
RAYLEIGH Kα
COMPTON Kβ
RAYLEIGH Kβ
17.42 keV
SCATTER PEAKS
Mo
XBL 767-8749

Fig. 5

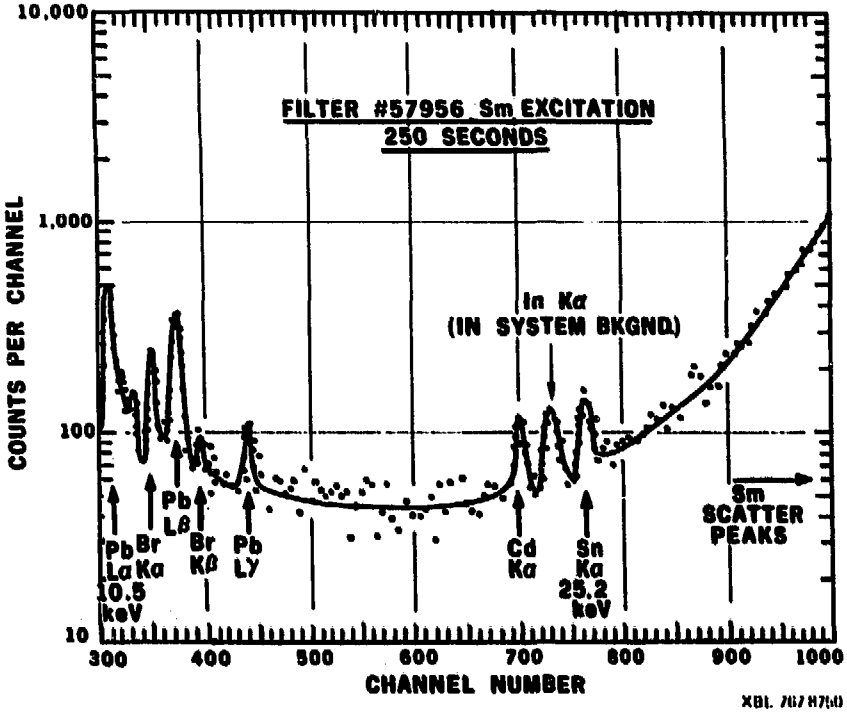
FILTER #57956 Sm EXCITATION
250 SECONDS
In Kα
(IN SYSTEM BKGND)
Sm
SCATTER
PEAKS
Pb
Lα
10.5
keV
Br
Kα
Pb
Lβ
Br
Kβ
Pb
Lγ
Cd
Kα
Sn
Kα
25.2
keV
COUNTS PER CHANNEL
CHANNEL NUMBER
10,000
1,000
100
10
300
400
500
600
700
800
900
1000
XBL 787-8760

Fig. 6

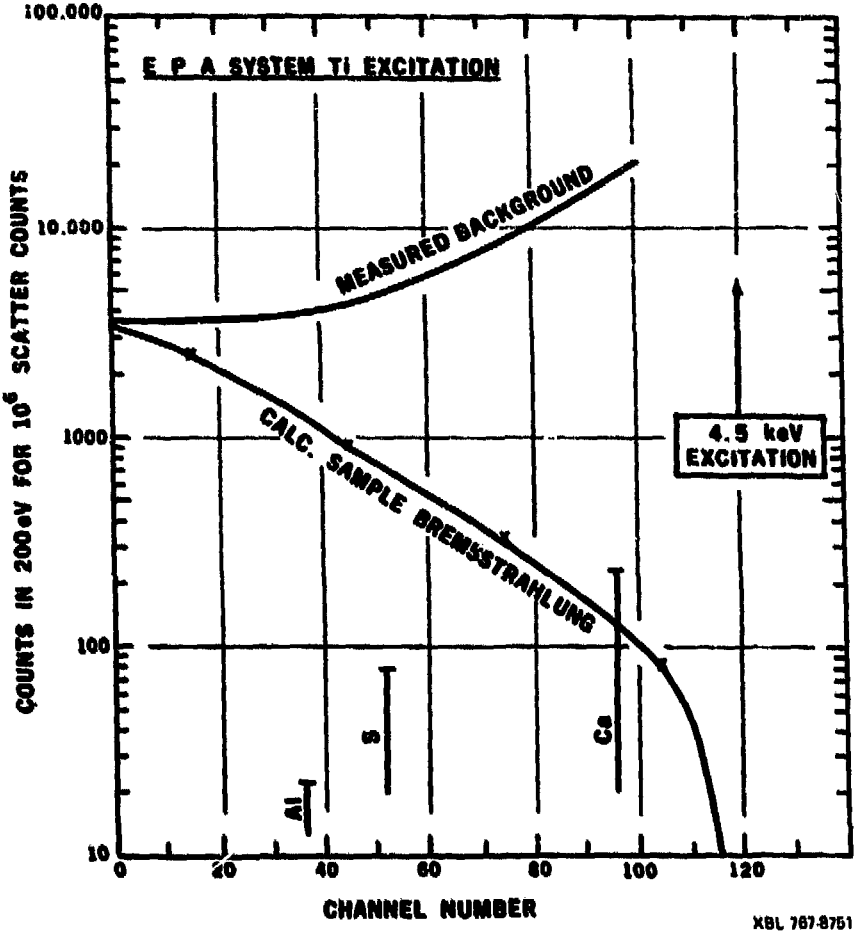
E P A SYSTEM Ti EXCITATION
MEASURED BACKGROUND
CALC. SAMPLE BREMSSTRAHLUNG
4.5 keV EXCITATION
Al
S
Ca
COUNTS IN 200eV FOR 10^6 SCATTER COUNTS
CHANNEL NUMBER
100,000
10,000
1000
100
10
0
20
40
60
80
100
120
XBL 767-8751

Fig. 7

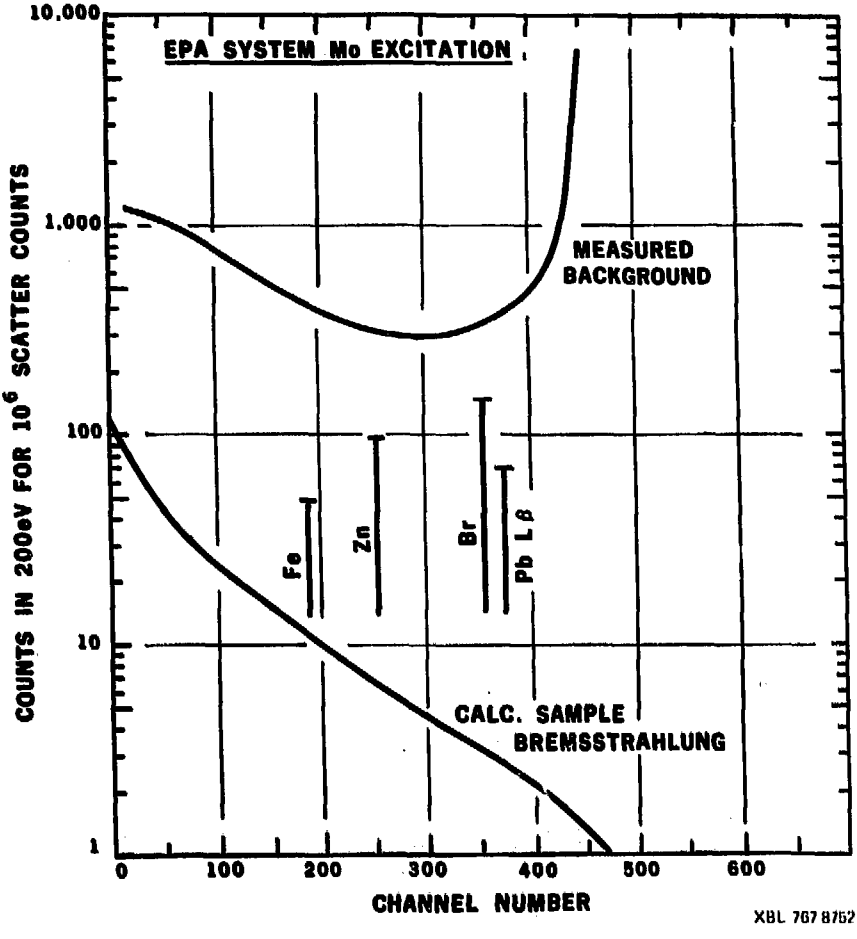
EPA SYSTEM Mo EXCITATION
MEASURED BACKGROUND
CALC. SAMPLE BREMSSTRAHLUNG
Fe
Zn
Br
Pb Lβ
COUNTS IN 200eV FOR 10^6 SCATTER COUNTS
CHANNEL NUMBER
10,000
1,000
100
10
1
0
100
200
300
400
500
600
XBL 767 8752

Fig. 8

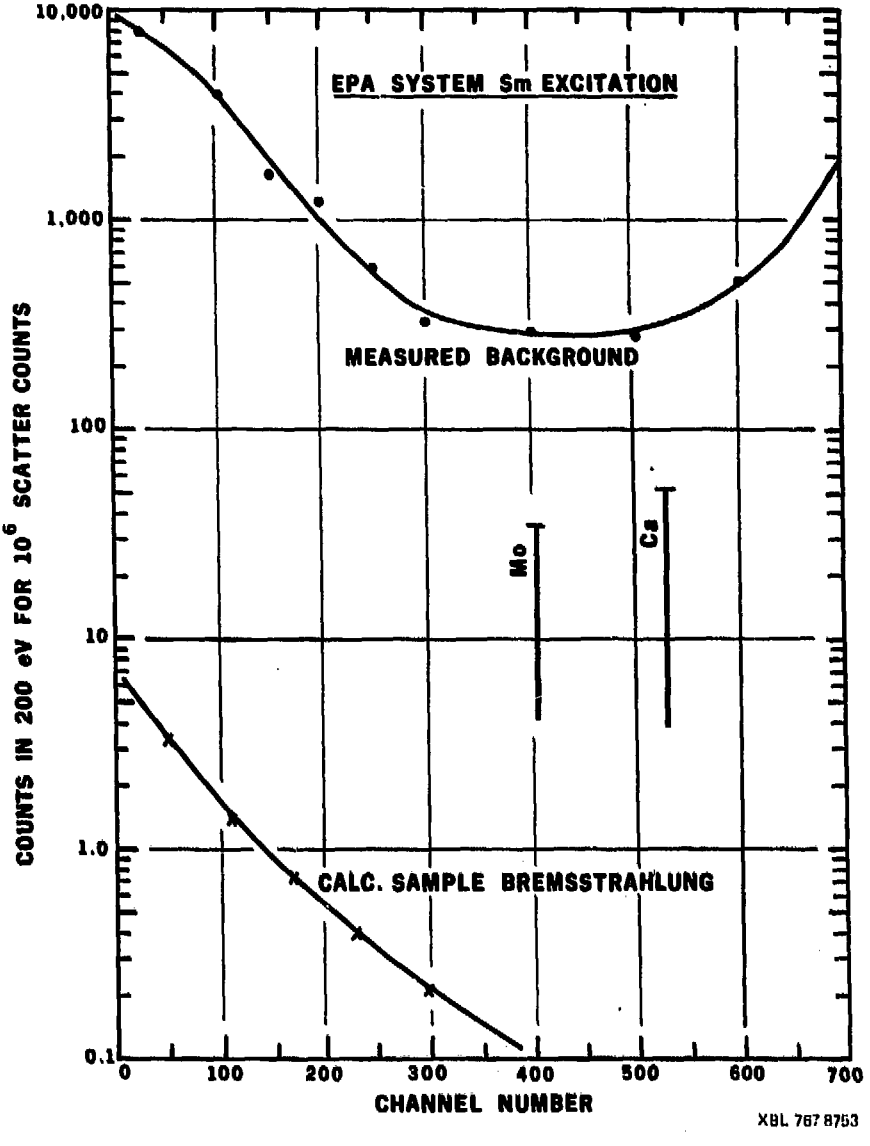
EPA SYSTEM Sm EXCITATION
MEASURED BACKGROUND
CALC. SAMPLE BREMSSTRAHLUNG
Mo
Ca
COUNTS IN 200 eV FOR 10^6 SCATTER COUNTS
CHANNEL NUMBER
10,000
1,000
100
10
1.0
0.1
0
100
200
300
400
500
600
700
XBL 767 8753

Fig. 9